

CERAMIC COATINGS FOR METALLIC COMPONENTS IN SUPERCRITICAL WATER-COOLED REACTORS

Francesco P. Orfino¹, Baisheng Yao¹, Yongsong Xie¹, Sing Yick¹, Jamie Miles², William Cook²,
and Rob Hui^{1*}

¹ Institute for Fuel Cell Innovation, National Research Council, 4250 Wesbrook Mall, Vancouver, BC, Canada, V6T 1W5

² Dept. Chemical Engineering, University of New Brunswick, PO Box 4400, Fredericton, NB, Canada, E3B 5A3

* Email: rob.hui@nrc-cnrc.gc.ca

Abstract

Zr-2.5Nb, a Zirconium alloy, cannot be used itself as a material of construction for SCWR applications, although it is desirable, from a neutron economy standpoint to use zirconium alloys for in-core materials. Thus, improving the oxidation resistance of zirconium through corrosion-resistant coatings is of interest for the SCWR. Plasma Electrolytic Oxidation (PEO) deposition was used to fabricate oxide coatings on Zr-2.5%Nb substrates from a sodium aluminate solution, which yielded an $\text{Al}_{(0.18)}\text{Zr}_{(0.82)}\text{O}_{(1.91)}$ coating. Spray Pyrolysis Deposition (SPD) was also used to fabricate Cr_2O_3 films on Zircaloy substrates. The samples were tested under supercritical water conditions (500°C, 25 MPa, deaerated) at exposure times of 100 and 250 hours. A reduction in corrosion rates of up to 50% at 100 hours of exposure, and up to 28% at 250 hours of exposure was noted. Both samples show improved corrosion resistance compared to the uncoated substrate.

1. Introduction

The supercritical water-cooled reactor (SCWR), which operates above the thermodynamic critical point of water (374 °C, 22.1 MPa), is an advanced concept for Generation IV nuclear reactors [1]. The SCWR has several advantages over current light water reactors (LWRs) including a much higher efficiency and smaller reactor footprints leading to improved economics and improved fuel utilization [1,2]. However, the increased efficiency requires much higher operating temperatures and pressures using supercritical water, which decreases the durability of typical materials used in this application. Under these conditions, the oxidation rate is increased, especially in the presence of dissolved oxygen [3].

Typical SCWR component materials should possess anti-corrosion properties in supercritical water at higher operating temperatures and pressures, as well as in oxidizing environments. Materials such as ferritic-martensitic stainless steels (F-M), nickel-, zirconium-, and titanium-based alloys, tantalum, noble metals or ceramics have been shown to be possible candidates with various degrees of resistance to the challenging conditions of SCWRs [3, 4]. Metals or alloys may be severely attacked under operating conditions of SCWRs, which offsets their advantages of high mechanical strength and easy fabrication into complex shapes. Alternatively, oxide ceramic materials, which offer better resistance in corrosive environments, may be coupled with an alloy substrate to offset

the disadvantages of metals or alloys alone [4-6]. Many techniques exist to deposit coatings on substrates as barriers against specific failure modes. In this work Spray Pyrolysis Deposition (SPD) and Plasma Electrolytic Oxidation (PEO) were used to manufacture such layers and their protective properties have been investigated under SCWR conditions.

The Spray Pyrolysis Deposition (SPD) technique is a simple and cost efficient method to coat metal oxides with protective coatings to improve corrosion resistance. Al_2O_3 , $(\text{Ta}_2\text{O}_5)_{0.04}(\text{CeO}_2)_{0.96}$ and $(\text{MgO})_{0.01}(\text{ZrO}_2)_{0.99}$ deposited by SPD on P91 have been corrosion tested in an autoclave under SCW conditions [5]. Of these oxides, Al_2O_3 on P91 showed significant corrosion protection ability; however, obtaining a crack free, dense SPD Al_2O_3 coating with a thickness greater than $5\mu\text{m}$ is difficult. Chromium oxide is able to provide a diffusion barrier against corrosion for stainless steel in a SCW environment by blocking further substrate oxidation [7]. In this study, Cr_2O_3 was selected for deposition on Zircaloy by SPD to investigate whether similar protection is noted.

Plasma Electrolytic Oxidation (PEO) has been shown to be an effective method of deposition for hard and corrosion resistant ceramic coatings on Al, Mg, Ti, Zr, and other light metals as well as their alloys [2, 8]. The properties of a PEO produced coating are its inherent high coating–substrate adhesion, its excellent wear and corrosion resistance, and its high thermal shock resistance coupled with its high hardness. These PEO coating properties, enhancing the materials' durability, are of particular interest for use in nuclear power plant applications. The essential concept behind this technique is the formation of a micro-arc plasma discharge on a sample surface while submerged in an aqueous electrolyte solution. The resultant oxide coating is typically composed of crystalline or amorphous phases ranging in thickness between $10\mu\text{m}$ to $50\mu\text{m}$ [9]. ZrO_2 as well as Al_2O_3 have been shown to form corrosion resistant coatings in a simulated SCW environment [5] and in this study, a PEO coating has been deposited on Zircaloy substrates and examined in an autoclave simulating the SCW environment.

2. Experimental section

2.1 Sample Preparation

Zr2.5Nb bars, ATI Wah Chang, were cut into specimens measuring $50\text{ mm} \times 10\text{ mm} \times 1\text{ mm}$ for PEO deposition and $20\text{ mm} \times 10\text{ mm} \times 1\text{ mm}$ for SPD. The former specimens were polished with a Struers RotoPol-35 polisher using MD Piano 220 then degreased with acetone followed by a rinse with de-ionized water, then air-dried. The latter specimens were polished with #400 SiC polishing paper, then cleaned in a sonicator with ethanol and air-dried.

A proprietary system for Plasma Electrolytic Oxidation (PEO) developed at NRC-IFCI [5, 10, 11] was used to produce protective oxide layers on Zr2.5Nb substrates. Each Zr2.5Nb substrate was placed in an electrolyte solution composed of an aqueous solution of 24.6 g L^{-1} sodium aluminate (NaAlO_2). A set of four PEO coatings were deposited with: $f = 1000\text{Hz}$, $D_{\text{pos}} = 20\%$, $D_{\text{neg}} = 10\%$, $R = 3:1$, $V_{\text{neg}} = 12\text{V}$, $V_{\text{pos}} = 550\text{V}$, a duration of *ca.* 20 minutes, and $I_{\text{MAX}} = 0.35\text{A}$ ($\sim 0.05\text{ A/cm}^2$); see Table 1. The coated samples were rinsed with de-ionized water and dried in air. The fourth sample (S4) was retained as a representative of the sample set for destructive characterization (SEM cross-sectioning) and was not tested in the autoclave. The PEO oxide coating thickness was measured by the eddy current technique (Oxford Instruments, Coating Measurement 200 Series). X-ray powder

diffraction was performed on a Bruker AXS D8 Advance with Cu K α radiation and used to deduce the protective oxide coating phase composition.

Table 1. Oxide coated samples details.

Sample ID	Coating Thickness (μm)	Technique	Comments
Zr-IFCI-1	20.0	PEO	Oxide coating; $J_1 = 49 \text{ mA/cm}^2$
Zr-IFCI-2	28.0	PEO	Oxide coating; $J_2 = 67 \text{ mA/cm}^2$
Zr-IFCI-3	16.0	PEO	Oxide coating; $J_3 = 43 \text{ mA/cm}^2$
S4	15.0	PEO	Oxide coating; $J_4 = 43 \text{ mA/cm}^2$
Zr-IFCI-4	~ 4	SPD	Cr ₂ O ₃ films
Zr-IFCI-5	~ 4	SPD	Cr ₂ O ₃ films
Zr-IFCI-6	~ 4	SPD	Cr ₂ O ₃ films

At IFCI, Scanning Electron Microscopy (SEM, Hitachi S-3500N, Japan) was employed to examine the PEO coatings' surface morphology as well as their cross-sections. Prior to SEM imaging of the surface, the samples were sputter coated (Polaron SC7640) with a thin layer of gold to minimize charging effects. The first step to prepare PEO cross-sectional samples was to nickel-plate them at 40 mA/cm^2 using a Dynatronix Inc. power supply and a Watts Ni solution containing $250 \text{ g/L NiSO}_4 \cdot 6\text{H}_2\text{O}$, 40 g/L boric acid, and $60 \text{ g/L NiCl}_2 \cdot 6\text{H}_2\text{O}$. The samples were each cut with a diamond saw (Buehler Isomet 2000) into two pieces each, which were hot mounted (Buehler Pneumet II) in an epoxy block. The resultant embedded samples were polished (Struers Rotopol-35) and gold coated prior to SEM examination. The coatings' chemical compositions and elemental distributions were analyzed by X-ray energy dispersion spectroscopy (EDS) from Oxford Instruments, which was attached to the SEM.

Spray Pyrolysis Deposition (SPD) utilized a precursor solution of $\text{Cr}(\text{NO}_3)_3$ supplied by a syringe pump with a specified flow rate. Compressed air provided a dynamic force to atomize the precursor solution through a spray nozzle and guided the atomized precursor solution to the heated substrate. After drying and thermal decomposition of the precursor near or at the surface of the Zr_{2.5}Nb, a Cr₂O₃ solid oxide layer was formed on the substrate surface. The substrate temperature was controlled at 650°C during SPD and the measured thickness of the resultant Cr₂O₃ films was about $4 \mu\text{m}$; see Table 1.

2.2 Exposure Tests

Supercritical water exposure tests were carried out in a flow loop at the University of New Brunswick. Figure 1(a) shows a piping and instrumentation diagram for the continuous flow system, which can operate with a range of conditions in both the subcritical and supercritical ranges. Deionized water from a reservoir (E-1) is pressurized with a positive displacement pump (P-1) to a pressure of 25 MPa. This water is initially heated with water returning from the system using a tube-in-tube interchanger (HX-1) with high temperature process fluid. The water is then heated (HX-2) through the critical point to the operating temperature of interest, in this study 500°C . Water then passes through an autoclave (E-2) in which the test coupons are suspended for exposure.

The hot fluid passes back through the tube-in-tube interchanger (HX-1) where some of its enthalpy is transferred to the incoming water. Before returning to the reservoir, the fluid is brought to ambient conditions by passing through a chilled water cooler (HX-3) and back-pressure regulating valve (BPRV-1).

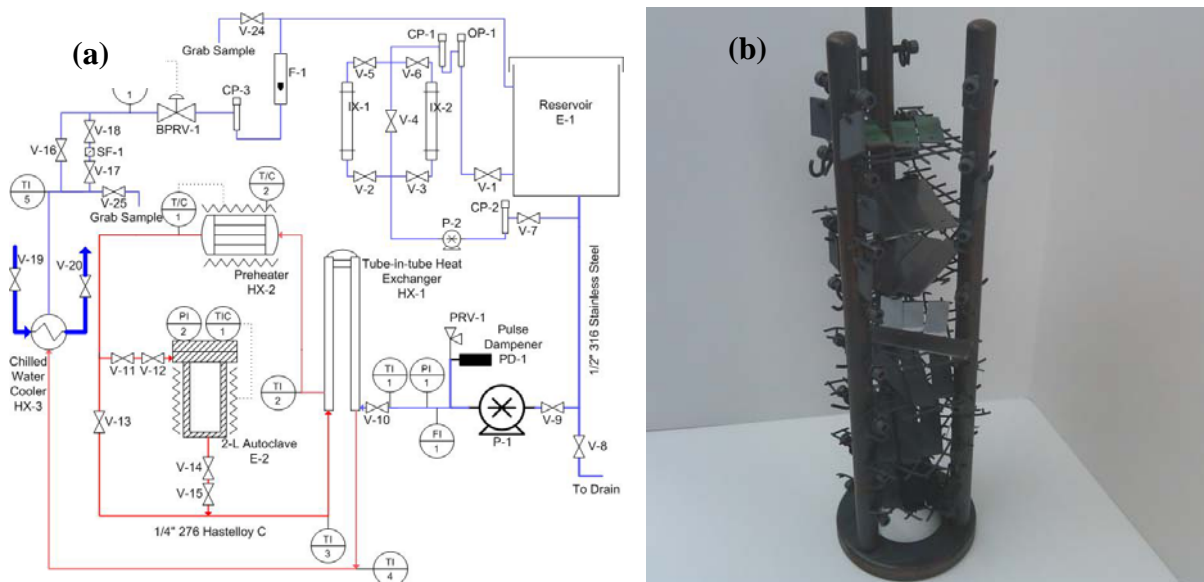


Figure 1. Details of autoclave testing system: (a) Schematic of UNB's SCW test loop and (b) Sample tree loaded with coupons.

As-received test coupons were placed on trays suspended from a tree, Figure 1(b), placed inside the autoclave and removed at intervals of approximately 100 and 250 hours to allow for SEM and weight change analyses to be carried out as a function of exposure time. For this experiment, the flow rate in the loop was fixed at 100 g/min with the dissolved oxygen concentration kept below 20 ppb as measured by an Orbisphere EC oxygen sensor in the water purification circuit.

The exposed coupons were characterized using scanning electron microscopy (SEM) at the Microscopy and Microanalysis Facility at the University of New Brunswick. Plan view images of the coated coupons were collected before and after exposure to evaluate the coating integrity. Secondary electron imaging (SEI) was performed on the coupons at increasing magnifications along with energy-dispersive x-ray spectroscopy (EDS) to obtain compositional information.

3. Results and discussions

During PEO coating deposition the average sample voltage was captured as a function of experimental time for each sample (Zr-IFCI-1 to Zr-IFCI-3) and is shown in Figure 2. These curves are characteristic of PEO in that initially, there is a sharp increase in voltage followed by a slowly increasing voltage. The initial rise in voltage is attributed to the formation of a passivating oxide layer on the substrate, which as the breakdown voltage is reached and sparks begin to occur, starts to break down. The breakdown voltage of *ca.* 300V is reached within the first minute for all samples while over the next 2 minutes when the voltage builds, the rate of sparking increases until the critical voltage of *ca.* 410V is reached and small sparks envelop the whole sample surface. The rest of the process time the voltage builds slowly and the sparks decrease in number but increase in

duration. The constant current applied and the varying oxide coverage shown in the optical samples images in Figure 2 yields differing current densities and non-superposition of the curves. The depositions were made in the current density range of 0.04 to 0.07 A/cm² and as the current densities increase the steepness of the initial voltage rise increases.

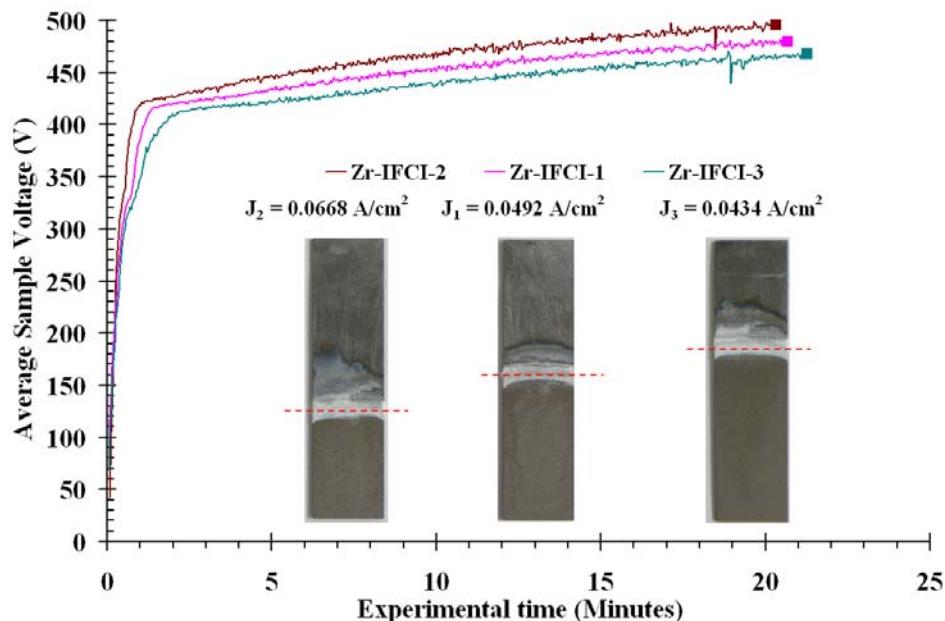


Figure 2. Voltage-Time response curves for PEO of Zircaloy substrates in 0.3 M solution of sodium aluminate at *ca.* 0.05 A/cm². The PEO deposition parameters were: 1000Hz, R = 3:1, $D_{\text{pos}} = 20\%$, $D_{\text{neg}} = 10\%$, $V_{\text{Max}} = 550\text{V}$, and $I_{\text{Max}} = 0.35\text{A}$. Optical images of the oxides on Zircaloy substrate that were autoclave tested are also shown.

SPD is essentially a continuous process, which allows coatings to be fabricated without any post processing steps. The SPD Cr₂O₃ coatings for this study (Zr-IFCI-4 to Zr-IFCI-6) were produced with a substrate heating temperature of 650°C. Representative SEM micrographs of the PEO and SPD oxide coating surfaces are shown in Figures 3(a) and 3(b), respectively. Figure 3(a) shows a characteristic series of pores, which are the micro channels left from the sparking events. There is also evidence of cracking throughout the surface imaged, interspersed among dense, annealed regions of oxide coating. Figure 3(b) shows that the resultant coatings are less dense than expected with a rather porous surface coating. Denser Cr₂O₃ coatings on Zr2.5Nb might be obtained by increasing the substrate heating temperature, as well as the dwell time, but the higher temperature and longer time heat treatment may damage the substrate.

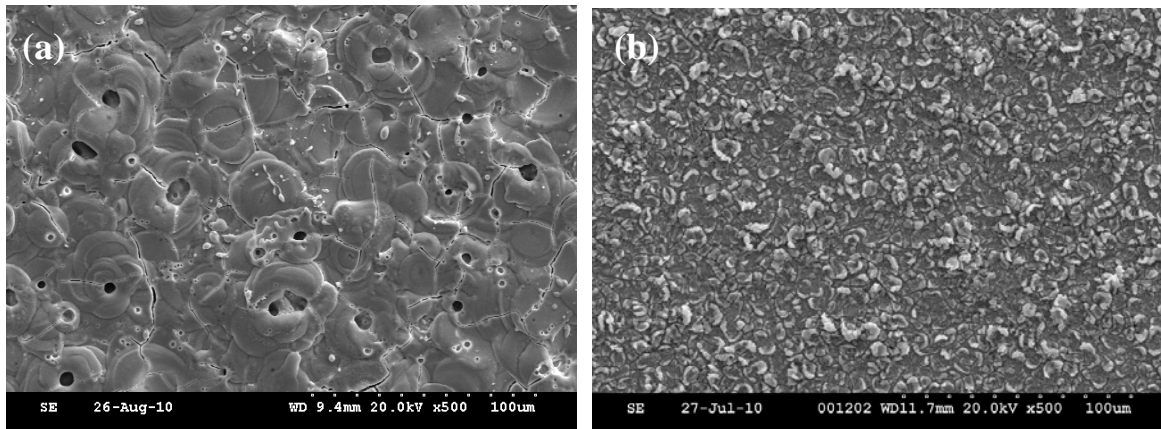


Figure 3. Representative surface SEM micrograph of: (a) the PEO coatings and (b) the SPD Cr₂O₃ coatings formed on Zr_{2.5}Nb substrates.

The corresponding XRD scan of the PEO sample to determine the phases of the oxide formed, as compared to the substrate, is shown in Figure 4 for sample S4. The Zr_{2.5}Nb substrate is well described by the Zr stick pattern. Similarly, the peaks corresponding to the PEO coating indicate that although some ZrO₂ peaks, as well as peaks from the Zr substrate, are detected, the coating consists mainly of Al_(0.18)Zr_(0.82)O_(1.91) (JCPDS No. 053-0572). The presence of much attenuated substrate peaks indicates that the PEO coatings are relatively thick.

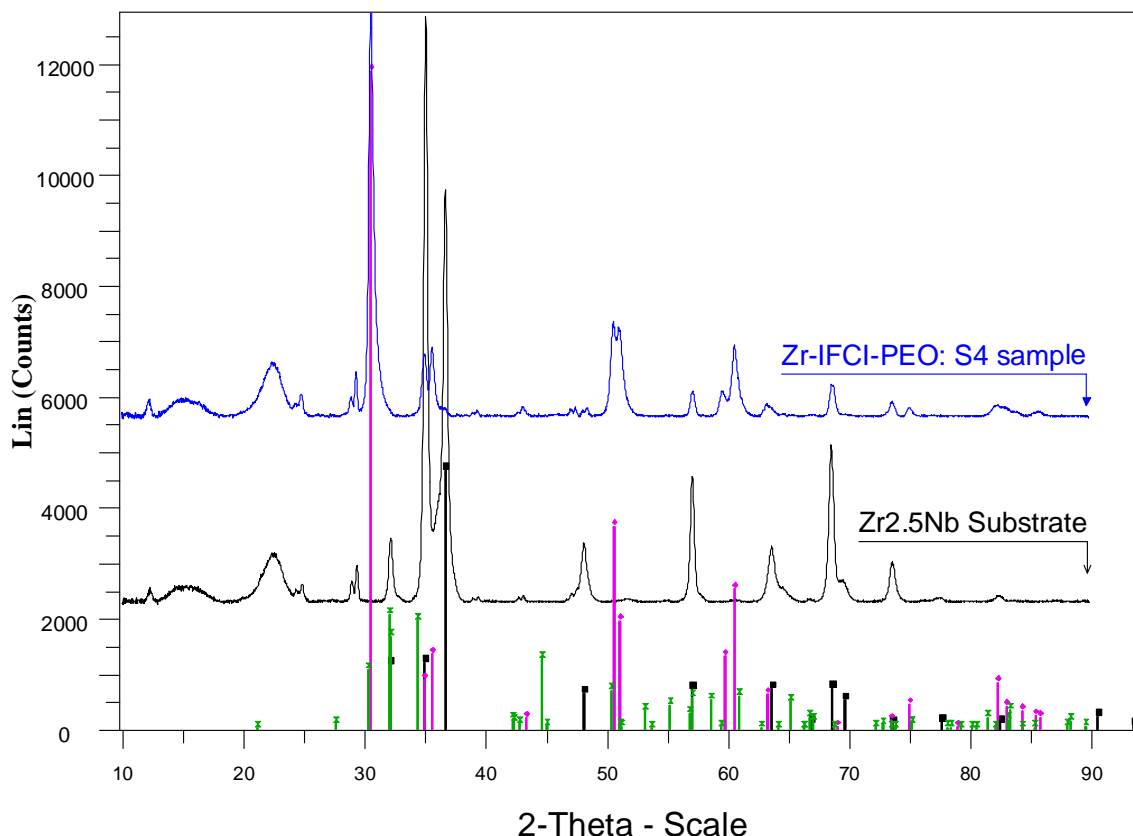


Figure 4. XRD patterns of the Zr_{2.5}Nb substrate and the PEO coated sample S4 deposited using PEO deposition parameters of: 1000Hz, R = 3:1, D_{pos} = 20%, D_{neg} = 10%, V_{Max} = 550V, and I_{Max} = 0.35A. The substrate and the coating peaks are attributed mainly to Zr and Al_(0.18)Zr_(0.82)O_(1.91) (JCPDS No. 053-0572).

The three PEO coated samples, whose optical images are shown in Figure 2, were cut along the red dotted lines shown and the oxide covered lower portions along with the SPD samples were autoclave tested. All the coated samples as well as bare substrates were exposed in neutral water in the SCW loop at 500°C, 25 MPa with low dissolved oxygen (~10 ppb); coupons were removed and weighed after 100 and 250 hours of exposure. All coated samples experienced nearly linear weight gains, as shown in Figure 5, while the uncoated Zr_{2.5}Nb substrates gained the most weight in the initial 100 hours; then, the rate of corrosion appears similar for all samples. These Zirconium-based coatings showed modest corrosion protection; i.e. reductions in corrosion rates up to 50% at 100 hours of exposure and up to 28% at 250 hours of exposure.

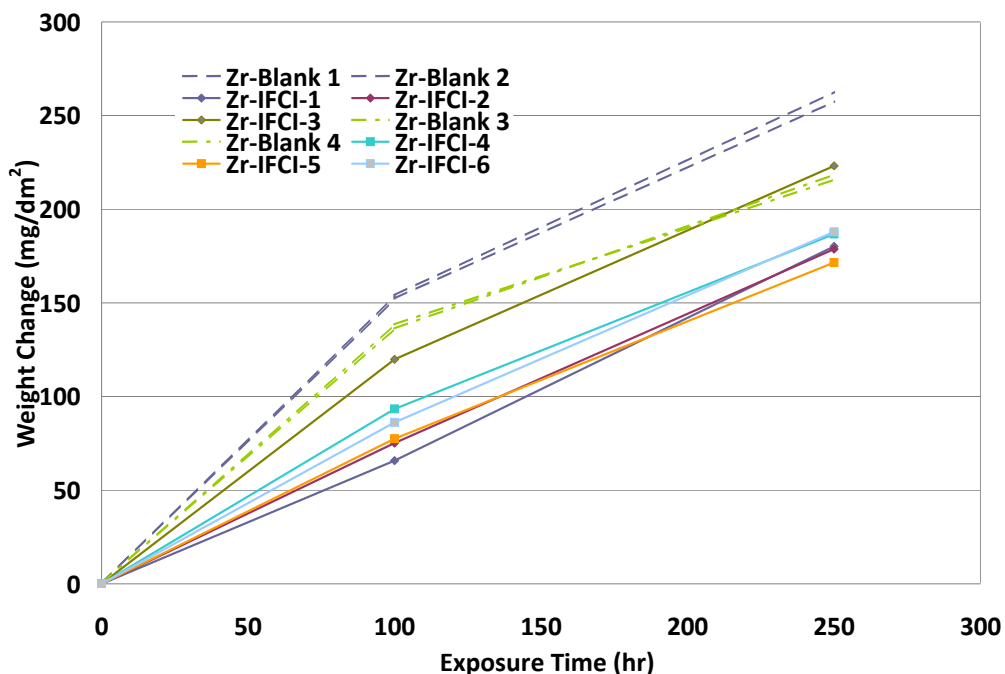


Figure 5. Weight change data for coated and uncoated Zr_{2.5}Nb coupons exposed to de-aerated SCW at 500°C and 25 MPa.

A likely cause of the decreasing degree of corrosion protection past the initial 100 hours for the PEO samples is that the coated samples were cut from the bare substrate, which left a section of bare Zr_{2.5}Nb exposed to the environment. Thus, the results convey information about the oxidation of the Zr-substrate as well as the protective capability of the oxide coating. Further, as exposure time increased more of the substrate under the oxide coating may have become more accessible to oxidation and manifested itself as increased substrate oxidation.

Plan view SEM images of the Zr_{2.5}Nb substrate, Zr-IFCI-1, and Zr-IFCI-5 samples before and after exposure are shown in Figure 6. Prior to exposure, the coated samples (Figure 6-c, e) show a porous and cracked morphology in the coating film while after exposure, some of the protective coating has been corroded away with some areas showing substrate sections (Figure 6-d, f). It is likely that these coating imperfections led to short-circuit pathways for the SCW to interact with the substrate material. Corrosion likely then went on unimpeded, contributing to the large weight gains observed that are comparable to the unprotected material. In fact, the slope of the curves on all the Zr samples are more-or-less the same after ~100 hours of exposure, indicating comparable oxidation rates on all samples and giving further evidence of relatively quick degradation of the coatings. Any protection that may have been present at shorter exposure times was most likely lost at the longer durations.

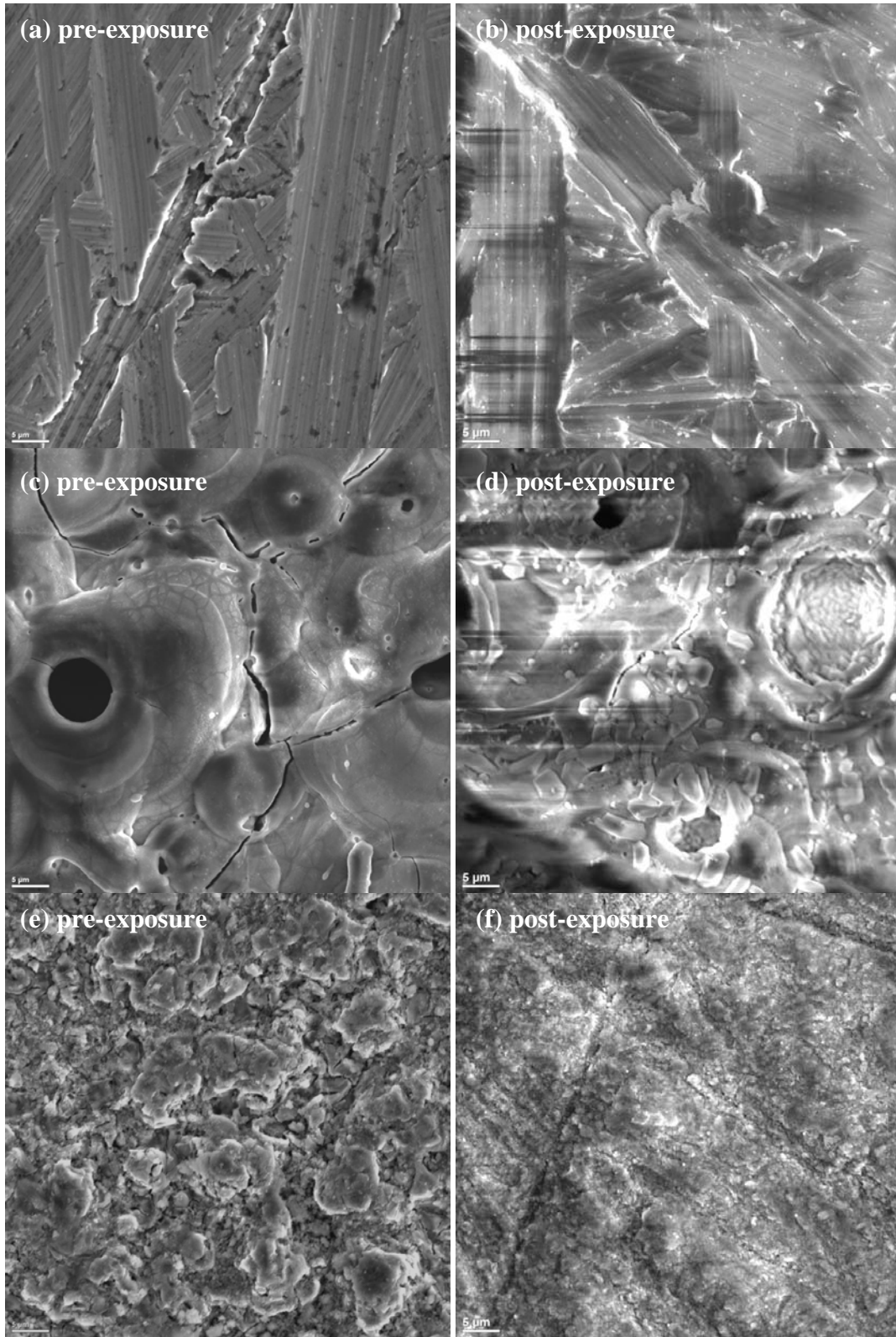


Figure 6. SEM images of uncoated Zr_{2.5}Nb (a), (b), Zr-IFCI-1 (c), (d), and Zr-IFCI-5 (e), (f) samples exposed to SCW at 500°C for 250 hours. The scale bar is 5 μm for all images.

Figure 7 shows representative cross-sectional images of the PEO samples and indicates that the coating is essentially composed of 3 sections: the first is a thin oxide layer adherent to the substrate of *ca* 2.5 μm thickness, the second is a porous layer close to the substrate (which may have pores or cracks connected to the surface) of *ca.* 10-12 μm thickness, and thirdly, a dense overlayer of *ca.* 3-6 μm thickness. Figure 7(b) shows a section where few pores or cracks are evident. This layered morphology indicates that in the initial period of testing, some degree of corrosion protection was available through the dense outer layer and the thinner substrate oxide base coating, as shown in Figure 5. Minimizing the surface pore diameter and decreasing the connectivity of the porous layer from the corroding fluid side to the substrate side would enhance that protection.

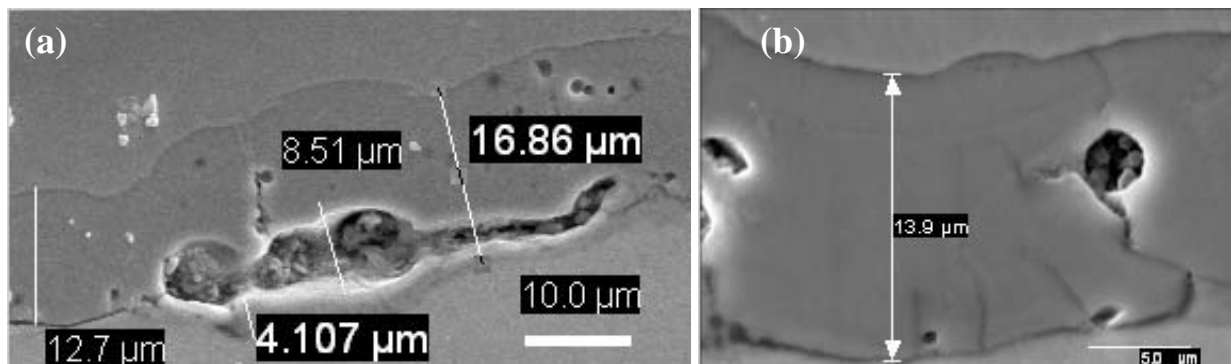


Figure 7. Representative SEM cross-sectional micrographs of the PEO coatings formed on Zr_{2.5}Nb substrates.

4. Conclusion

$\text{Al}_{(0.18)}\text{Zr}_{(0.82)}\text{O}_{(1.91)}$ coatings fabricated by PEO and Cr_2O_3 coatings fabricated by SPD all on Zr_{2.5}Nb substrates were tested in a flow loop by exposure to supercritical water at 500°C, 25 MPa with low dissolved oxygen (~10 ppb). Weighing the samples and calculating the weight gain/loss quantified oxidation at 100 hours and 250 hours. Ceramic-coated Zr_{2.5}Nb substrates prepared by PEO and SPD showed some initial protection against corrosion when compared to the uncoated Zr_{2.5}Nb samples; large weight gains were observed for all coupons and the coatings were shown in SEM work to deteriorate over time. For better protection, these coatings should be denser and thicker, which can be achieved by optimizing deposition parameters. Additionally, exposure tests on samples without a cut edge would decouple the effect of substrate oxidation from coating corrosion effects.

5. Acknowledgment

The authors acknowledge the financial support from the Canadian National Program on Generation IV Energy Technologies, the NSERC/NRCan/AECL Generation IV Technologies Program.

6. References

- [1] “A Technology Roadmap for Generation IV Nuclear Energy Systems”, U.S. DOE Nuclear Energy Research Advisory Committee and the Generation IV International Forum, Report No. GIF-002-00, Dec 2002
- [2] S. Baidur, “Materials challenges for the Supercritical Water-Cooled Reactor (SCWR)”, *Bulletin of the Canadian Nuclear Society*, 29 (2008) 32-38
- [3] G.S. Was, P. Ampornrat, G. Gupta, S. Teyseyre, E.A. West, T.R. Allen, Sridharan, L. Tan, Y. Chen, X. Ren, C. Pister, “Corrosion and stress corrosion cracking in supercritical water”, *J. Nucl. Mater.* 371 (2007) 176-201
- [4] C.W. Sun, R. Hui, W. Qu, S. Yick, “Progress in corrosion resistant materials for supercritical water reactors”, *Corros. Sci.* 51 (2009) 2508-2523
- [5] D.A. Guzonas, J.S. Wills, G.A. McRae, S. Sullivan, K. Chu, K. Heaslip, M. Stone, “Corrosion-Resistant Coatings For Use in a Supercritical Water CANDU[®] Reactor”, *Proc. 12th Int. Conf. on Env Degradation of Materials in Nuclear Power System – Water Reactors*, (2005) 1379-1385
- [6] R. Hui, W. Cook, C. Sun, Y. Xie, P. Yao, J. Miles, R. Olive, J. Li, W. Zheng, and L. Zhang, “Deposition, Characterization and Performance Evaluation of Ceramic Coatings on Metallic Substrates for Supercritical Water-cooled Reactors”, *Surf. & Coat. Technol.*, in press (2010)
- [7] L. Zang, F. Zhu and R. Tang, “Corrosion mechanisms of candidate structural materials for supercritical water-cooled reactor”, *Front. Energy Power Eng. (China)*, 3 (2009). 233–240
- [8] A.L. Yerokhin, X. Nie, A. Leyland, A. Matthews, S.J. Dowey, “Plasma electrolysis for surface engineering”, *Surf. and Coat. Technol.* 122 (1999) 73-93
- [9] E. Matykina, P. Skeldon, G.E. Thompson, “Fundamental and practical evaluation of plasma electrolytic oxidation coatings of titanium”, *Surf. Eng.* 23 (2007) 412–418.
- [10] PCT/CA2010/000987, “Novel pulsed power supply for plasma electrolytic deposition and other processes”, filed 06/08/2010
- [11] C.W. Sun, R. Hui, W. Qu, S. Yick, C Sun, W. Qian, “Effects of processing parameters on microstructures of TiO₂ coatings formed on titanium by plasma electrolytic oxidation”, *J. Mater. Sci.* 45 (2010) 6235-6241, DOI: 10.1007/s10853-010-4718-7